Published in final edited form as:
J Magn Reson Imaging. 2014 July ; 40(1): 13–25. doi:10.1002/jmri.24333.

Clinical Performance of Contrast Enhanced Abdominal Pediatric MRI with Fast Combined Parallel Imaging Compressed Sensing Reconstruction

Tao Zhang, MS[*,1], **Shilpy Chowdhury, MD, MPH**[*,2], **Michael Lustig, PhD**[3], **Richard A. Barth, MD**[2], **Marcus T. Alley, PhD**[2], **Thomas Grafendorfer, MS**[4], **Paul D. Calderon, MS**[5], **Fraser J.L. Robb, PhD**[6], **John M. Pauly, PhD**[1], and **Shreyas S. Vasanawala, MD, PhD**[2]

[1]Electrical Engineering, Stanford University, Stanford, California, USA

[2]Radiology, Stanford University, Stanford, California, USA

[3]Electrical Engineering and Computer Sciences, University of California, Berkeley, California, USA

[4]GEHC Coils, GE Healthcare, Stanford, California, USA

[5]Hardware Engineering, GE Healthcare, Fremont, California, USA

[6]GE Healthcare, Aurora, Ohio, USA

Abstract

Purpose—To deploy clinically, a combined parallel imaging compressed sensing method with coil compression that achieves a rapid image reconstruction, and assess its clinical performance in contrast-enhanced abdominal pediatric MRI.

Materials and Methods—With IRB approval and informed patient consent/assent, 29 consecutive pediatric patients were recruited. Dynamic contrast-enhanced MRI was acquired on a 3T scanner using a dedicated 32-channel pediatric coil and a 3D SPGR sequence, with pseudo-random undersampling at a high acceleration (R=7.2). Undersampled data were reconstructed with three methods: a traditional parallel imaging method and a combined parallel imaging compressed sensing method with and without coil compression. The three sets of images were evaluated independently and blindly by two radiologists at one siting, for overall image quality and delineation of anatomical structures. Wilcoxon tests were performed to test the hypothesis that there was no significant difference in the evaluations, and inter-observer agreement was analyzed.

Results—Fast reconstruction with coil compression did not deteriorate image quality. The mean score of structural delineation of the fast reconstruction was 4.1 on a 5-point scale, significantly better ($P<0.05$) than traditional parallel imaging (mean score 3.1). Fair to substantial inter-observer agreement was reached in structural delineation assessment.

Correspondence to: Tao Zhang, Packard 208, 350 Serra Mall, Stanford, CA 94305, Phone: (650) 725-5638, Fax: (650) 723-8374, tao@mrsrl.stanford.edu.
*The two authors contributed equally.

Conclusion—A fast combined parallel imaging compressed sensing method is feasible in a pediatric clinical setting. Preliminary results suggest it may improve structural delineation over parallel imaging.

Keywords

Contrast-enhanced abdominal pediatric MRI; Coil compression; Parallel imaging; Compressed sensing

INTRODUCTION

There are several challenges in pediatric body MRI: the inherently small anatomy requires an MR acquisition with a very high spatial resolution; the nature of rapid hemodynamics in pediatric patients requires imaging quickly for contrast-enhanced MRI (1-3); and fast breathing and voluntary motion cause several artifacts, so anesthesia is usually needed (4). Thus, imaging speed is critical to more widespread use of pediatric abdominal MRI.

To significantly accelerate MR acquisition, two types of approaches are usually considered. The first type is known as parallel imaging (PI) (5,6). PI uses a set of phased array coils (7) with different coil sensitivities for collecting data. The coil sensitivities are used to accelerate MR data acquisition by undersampling *k*-space and to reconstruct the missing data. The second type is compressed sensing (CS), which has been developed more recently (8). CS exploits the data redundancy (also known as sparsity) in MR images (9), which essentially requires less data to be acquired. A nonlinear optimization method is often used to reconstruct the undersampled data. Furthermore, the combination of PI and CS can achieve even faster imaging (10-12). Compared to the traditional Fourier transform used for Cartesian imaging at the Nyquist sampling rate, the complexity and computation time of a PI and CS reconstruction is dramatically increased (13,14). Most PI and combined parallel imaging compressed sensing methods have reconstruction time proportional to as much as the third order of the number of coils. Dedicated high-density coils can push the limits of acceleration factors (15-17). However, the challenge of the long image reconstruction time is even more significant. The lengthy reconstruction (usually varying from several minutes up to a few hours) is not practical in a clinical setting, where image quality must be confirmed prior to either awakening a child from anesthesia or releasing a patient from the imaging suite. This is particularly true for contrast-enhanced imaging.

Coil compression (CC) has been proposed to reduce the computation for large coil arrays (18-20). The original data from many coils can be combined into few virtual coils, on which the reconstruction is performed. As a result, the reconstruction time can be significantly shortened because of the reduced number of virtual coils (20). While this may enable the application of PI and CS with high acceleration in a clinical setting, it may also alter the reconstructed images, effecting clinical performance.

In this work, we focus on the clinical deployment of a combined parallel imaging compressed sensing technique with rapid image reconstruction and the assessment of the resulting image quality. We implement a combined parallel imaging compressed sensing method, namely L_1-SPIRiT (21), with a CC (20) algorithm to enable fast image

reconstruction. We investigate the clinical performance of the combined parallel imaging compressed sensing technique with coil compression in contrast-enhanced abdominal pediatric MRI.

MATERIALS AND METHODS

Patient Recruitment

With institutional review board approval and informed patient consent and/or assent, 29 consecutive patients (14 males and 15 females) referred for contrast-enhanced abdominal MRI under anesthesia at our institution with concern of inflammation (3 cases) or for tumor surveillance (26 cases) were recruited from September 2010 to May 2011. Patient demographics are summarized in Table 1, with ages ranging from 3 months to 9 years (mean, 3.79 years).

Image Acquisition

All imaging was performed on a 3T MR750 MRI scanner (GE Healthcare, Waukesha, WI, USA) with a dedicated 32-channel pediatric custom phased array coil that consisted of a pair of 4-by-4 array coils, one positioned posterior and the other anterior to the abdomen (15). A 3D spoiled gradient echo sequence with intermittent fat suppression was modified to incorporate variable density Poisson-disc *k*-space sampling (22), which facilitates compressed sensing by ensuring relatively incoherent aliasing artifacts from *k*-space undersampling. Prescribed acquisition parameters were echo time (TE) 0.7-1.09 ms, repetition time (TR) 3.6-4.4 ms, bandwidth (BW) 128 kHz, slice thickness 0.8-1mm, FOV 24-32 cm, in-plane matrix 288×288 or 320×320 (shown in Table 1), and a total acceleration factor of 7.2. The average acquisition time for each temporal phase was 22.9 seconds (range, 19.5-27.6 seconds). One pre-contrast and up to four post-contrast acquisitions were performed. Single dose gadobenate dimeglumine was diluted as necessary in saline to ensure a volume of at least 10 mL and power injected intravenously at 1mL/sec rate for all but one patient. The remaining one patient was injected with a single dose gadofosveset trisodium, again diluted in saline to a volume of 10 mL and power injected at 1mL/sec rate.

Image Reconstruction

For each subject, three image reconstructions of the arterial phase data were performed. The first reconstruction was a traditional parallel imaging reconstruction with the commercially available Autocalibrating Reconstruction for Cartesian imaging (ARC) algorithm (23). The second reconstruction was L_1-SPIRiT reconstruction, which is a combination of autocalibrating parallel imaging and compressed sensing. The third reconstruction was the coil compressed L_1-SPIRiT (CC-L_1-SPIRiT), which is the combination of L_1-SPIRiT with coil compression (CC) (19).

For the third reconstruction, the original 32 coils were combined into 6 virtual coils before L_1-SPIRiT reconstruction was performed. In the second and third reconstructions, L_1-SPIRiT was performed using a projection onto convex set (POCS) algorithm (21) and a fixed 50 iterations were set as the point of convergence. In this iterative reconstruction, a soft-thresholding operation in the Wavelet domain was carried out. The Wavelet threshold

was chosen empirically: for L_1-SPIRiT, the threshold was initialized with 0.05 and gradually decreased to 0.0002 as the number of iterations increased; for CC-L_1-SPIRiT, the threshold was fixed at 0.0025 for all iterations. Note that the image quality of L_1-SPIRiT heavily depends on the chosen Wavelet threshold (14). An inaccurate threshold would introduce artifacts in the reconstructed images, such as image blurring or synthetic appearance. When these image artifacts appeared in the reconstruction with the default parameter, a case-specific parameter tuning was performed. Prior to the L_1-SPIRiT reconstruction, the data were normalized such that the maximum value in a zero-filled reconstruction was one in order to guarantee that the wavelet thresholding parameter was independent of the scaling of the data.

Image Evaluation

Two board-certified pediatric radiologists (reader 1 and 2 with 8 and 23 years of clinical experience with pediatric MR imaging respectively) who were blinded to the types of reconstructions and patient history/diagnoses independently assessed image qualitatively. First, images were assessed for their overall image quality including qualitative signal-to-noise ratio (SNR), image contrast, synthetic appearance, coherent structural artifacts and image blurring. The scoring criteria are listed in Table 2. Here, synthetic appearance refers to the subjective somewhat “cartoon-like” artificial appearance, sometimes seen in compressed sensing reconstructions. Based on the overall image quality scores, the reconstructed images were considered to be diagnostically acceptable or non-acceptable (shown in Table 2). Then the quality of delineation of several anatomical structures (renal arteries, liver, portal veins, hepatic veins, pancreas, adrenals and spine) that are routinely assessed on these abdominal MRI exams was graded on the pre-defined criteria listed in Table 3. The reconstructions were first presented to the radiologists individually in a blinded fashion and randomized order, and then presented in pairs for direct side-by-side comparison, again in blinded randomized order. For side-by-side paired comparison, the radiologists were also asked for preference of the delineation of anatomical structures based on the criteria shown in Table 4. When present, the quality of delineation of pathologic lesions was also evaluated for paired comparison. The delay time between the reading sessions was more than one month.

Statistical Analysis of Overall Image Quality—The assessed images were first divided into two groups based on the scores: diagnostically acceptable and non-acceptable. The percentage of the number of cases that were diagnostically acceptable was calculated for each reconstruction. Then, a paired Wilcoxon test was performed to assess the null hypothesis that there was no significant difference in image quality between ARC and L_1-SPIRiT, ARC and CC-L_1-SPIRiT, and L_1-SPIRiT and CC-L_1-SPIRiT, when assessed individually, for qualitative SNR, image contrast, synthetic appearance, coherent structural artifacts and image blurring.

Statistical Analysis of Delineation of Specific Abdominal Anatomical Structures

Individual assessments: A paired Wilcoxon test was performed to assess the null hypothesis that there was no significant difference in image quality between ARC and L_1-

SPIRiT, ARC and CC-L_1-SPIRiT, and L_1-SPIRiT and CC-L_1-SPIRiT, when images were assessed individually for anatomical structures (renal arteries, liver, hepatic veins, portal veins, pancreas, adrenals, and spine). For the seven tests of anatomical structural delineation, a Benjamini-Hochberg multiple comparison correction was also applied to adjust to the statistical significance level.

Paired comparisons: For evaluations with images shown side-by-side in pairs, a paired Wilcoxon test was performed to assess the null hypothesis that there was no significant preference in quality of structural delineation between ARC and L_1-SPIRiT, ARC and CC-L_1-SPIRiT, and L_1-SPIRiT and CC-L_1-SPIRiT.

In all the aforementioned analysis, a P value of 0.05 was used as a criterion of statistical significance. Inter-observer agreements between the two readers for all qualitative image assessments and delineation of anatomical structures were analyzed using bi-rater weighted kappa coefficients. The weighted kappa coefficients were interpreted as almost perfect (0.8-1), substantial (0.6-0.8), moderate (0.4-0.6), fair (0.2-0.4), slight (0-0.2) and poor (<0).

RESULTS

Reconstruction time for each acquisition (each temporal phase) with CC-L_1-SPIRiT ranged from 28-48 seconds (mean, 36 seconds) compared to 202-364 seconds with L_1-SPIRiT (mean, 275 seconds), for nearly an eight-fold reduction in image reconstruction time. This reconstruction time of less than one minute is acceptable for clinical use, even when resulting images have to be inspected to confirm adequate image quality prior to releasing the patient. The reconstruction time for each case is shown in Tab. 1. Figure 1 shows a representative results in a 6-year-old female referred for abdominal pain and concern for inflammatory bowel disease, and highlights the overall improvement in image quality with a compressed sensing reconstruction.

Individual Assessment Of Overall Image Quality

SNR—Results for all qualitative image assessments are detailed in Table 5 and 6. For reader 1, all cases had diagnostically acceptable qualitative SNR with L_1-SPIRiT and CC-L_1-SPIRiT reconstructions. For reader 2, 27/29 and 28/29 cases had diagnostically acceptable SNR for L_1-SPIRiT and CC-L_1-SPIRiT, respectively. With ARC reconstruction, non-acceptable SNR was present in 13/29 cases for reader 1 and 11/29 cases for reader 2.

Image Contrast—All cases had diagnostically acceptable image contrast with ARC, L_1-SPIRiT and CC-L_1-SPIRiT reconstructions for reader 1. For reader 2, the proportion of cases with significant degradation of image contrast progressively decreased from ARC reconstruction to L_1-SPIRiT and finally CC-L_1-SPIRiT, with at least 90% of cases having acceptable image contrast for all CS reconstructions.

Synthetic Appearance—None of the cases with ARC had a significant synthetic appearance for both reader 1 and reader 2. However, for reader 1, a significant synthetic appearance was seen in three cases with L_1-SPIRiT and five cases with CC-L_1-SPIRiT. Similarly for reader 2, synthetic appearance was present in one case with CC-L_1-SPIRiT

reconstruction. Figure 2(b) shows an example of synthetic appearance in L_1-SPIRiT reconstruction. However, the synthetic appearance in the reconstructed images depends significantly on the reconstruction parameters (e.g., Wavelet threshold). By adjusting the reconstruction parameters, synthetic appearance can be removed as shown in Figure 2(c).

Coherent Structural Artifacts—For reader 1, all 29/29 cases had either no or minimal structural coherent artifacts with ARC, L_1-SPIRiT and CC-L_1-SPIRiT reconstructions. Since all three reconstructions were acquired using Poisson disc pseudo-random *k*-space sampling, coherent structural artifacts were neither present nor expected. Similarly, for reader 2, all 29/29 cases had no or minimal structural coherent artifacts with ARC and CC-L_1-SPIRiT reconstructions. However, structural artifacts were present in two cases with L_1-SPIRiT.

Image Blurring—For reader 1, each of the three reconstructions had one case with a non-diagnostic degree of blurring, which was influenced by motion. For reader 2, the proportion of cases with a significant degree of blurring decreased progressively from ARC (41%) to L_1-SPIRiT (17%) and then CC-L_1-SPIRiT (10%) reconstruction.

Aside from the analysis that was focused on the proportion of cases with a diagnostically acceptable image quality, comparisons of qualitative image assessments between ARC and L_1-SPIRiT, ARC and CC-L_1-SPIRiT, and L_1-SPIRiT and CC-L_1-SPIRiT, when assessed individually are detailed in Table 6. Figures 3 shows representative results of blinded randomized scoring of overall qualitative image assessments. From Table 6, we can see that both L_1-SPIRiT and CC-L_1-SPIRiT have a statistically significant difference compared with ARC when assessed individually (paired Wilcoxon rank sum test, $P<0.05$) in qualitative SNR, coherent structural artifacts and synthetic appearance for both readers. Similar statistically significant difference is also achieved in image contrast and image blurring for reader 2, but not for reader 1. L_1-SPIRiT and CC-L_1-SPIRiT do not have a statistically significant difference in overall image quality for both readers except in synthetic appearance for reader 1.

Delineation Of Specific Abdominal Anatomical Structures

Individual Assessment—Delineation for all anatomical structures except the renal artery was superior with both L_1-SPIRiT and CC-L_1-SPIRiT reconstructions compared with ARC (paired Wilcoxon rank sum test, $P<0.05$) for both readers. However, no statistically significant difference was found between L_1-SPIRiT and CC-L_1-SPIRiT reconstructions for delineation of all anatomical structures for reader 1 or reader 2, as detailed in Table 6. Figure 4 shows representative results of blinded randomized order scoring of delineation of renal arteries, liver, portal veins, hepatic veins, pancreas, adrenals, and spine with ARC, L_1-SPIRiT, and CC-L_1-SPIRiT reconstructions for both readers. After the Benjamini-Hochberg multiple comparison correction, statistical significance was still achieved to reject the null hypothesis that there was no significant difference in image quality between ARC and L_1-SPIRiT, and ARC and CC-L_1-SPIRiT for all anatomical structures except the renal artery.

Paired Comparisons—Delineation of all anatomical structures was superior with L_1-SPIRiT and CC-L_1-SPIRiT compared with ARC for each reader, as summarized in Table 7.

Further, for reader 1, there was no clear preference for L_1-SPIRiT or CC-L_1-SPIRiT when compared against each other for most structures. Reader 2 preferred CC-L_1-SPIRiT for some anatomical structures (renal artery, portal vein, pancreas, adrenals and spine) and had no strong preference between L_1-SPIRiT and CC-L_1-SPIRiT in the other anatomical structures. The Wilcoxon test results are also shown in Table 7. The comparisons of all seven structures were combined and the results were illustrated using bar graphs in Fig. 5. Again, CC-L_1-SPIRiT had superior or equivalent structural delineation compared to ARC for all comparisons and both readers (Fig. 5 (c, d)).

In our study cohort, 24 patients had pathological lesions. For reader 1, delineation of lesions was superior with L_1-SPIRiT reconstruction compared with ARC in all cases, and was superior in 23/24 cases with CC-L_1-SPIRiT compared with ARC. For reader 2, delineation of lesions was superior in 14/24 cases with L_1-SPIRiT compared with ARC and in 16/24 cases with CC-L_1-SPIRiT compared with ARC. For reader 2, the difference between L_1-SPIRiT and ARC as well as between CC-L_1-SPIRiT and ARC for delineation of lesions again showed a significant improvement with compressed sensing, but not as strongly as with reader 1.

Inter-observer Agreement—Overall inter-observer agreement for image qualitative assessments and delineation of specific anatomical structures are shown in Table 8. Two readers had fair to substantial agreement for most delineation of specific anatomical structures with ARC, L_1-SPIRiT and CC-L_1-SPIRiT. However, the agreement on overall image quality assessments was not as good as structural delineation because the scoring criteria for overall image quality were more subjective.

DISCUSSION

This work addresses some of the challenges of pediatric MR imaging by leveraging a compressed sensing approach to double the speed of contrast-enhanced abdominal MRI. The study showed that compressed sensing, when combined with a fast image reconstruction method, is feasible in a pediatric clinical setting. Delineation of anatomical structures that are routinely evaluated in a clinical setting shows improved quality with a compressed sensing reconstruction, and further, coil compression does not adversely affect image quality. The results of individual overall image quality assessment suggest that a compressed sensing reconstruction will yield diagnostically acceptable SNR that is unlikely to be achieved by a parallel imaging alone. Image contrast degradation, image blurring and coherent structural artifacts are unlikely to be seen in a compressed sensing reconstruction. The results of side-by-side comparison show that compressed sensing reconstructions are likely to provide superior structural delineation than traditional parallel imaging and that accelerated image reconstruction via coil compression can be accomplished with no significant image degradation.

In this study, the average reconstruction time for combined parallel imaging compressed sensing method without coil compression is approximately 275 seconds. In a typical contrast-enhanced abdominal imaging setting, one pre-contrast and up to four post-contrast acquisitions are usually acquired. As a result, the whole image reconstruction takes up to

approximately 23 minutes. This is not practical in a clinical setting where image quality needs to be confirmed before patients are released. However, when coil compression is applied, the entire reconstruction time is reduced to less than 3 minutes. If receiving coils with higher channel counts (more than 32) are used, the reconstruction time will increase even further. However, arguably for the same acquisition, the number of virtual coils needed may not increase dramatically. Thus, a practical reconstruction time will be maintained.

The combined parallel imaging compressed sensing reconstructions (L_1-SPIRiT and CC-L_1-SPIRiT) implemented in this work were parameter-dependent. The parameters used in the study were chosen empirically and were fixed for all the cases. Synthetic appearance may appear in the image due to the fixed non-optimal reconstruction parameters for specific cases. However, it can be removed by properly adjusting the reconstruction parameters. In general, the reconstruction parameters applied in this study provided at least 90% of reconstructions without obvious synthetic appearance. Reconstructions with an automatic parameter selection may completely remove the synthetic appearance in the reconstructed images, but are beyond the scope of this manuscript.

Overall, we did not find much difference in image quality between L_1-SPIRiT (compressed sensing) and CC-L_1-SPIRiT (compressed sensing and coil compression) reconstructions, though images obtained with CC-L_1-SPIRiT showed superior quality for some overall image qualitative assessments and delineation of anatomical structures, compared with L_1-SPIRiT. However, CC-L_1-SPIRiT increased the synthetic appearance of images while decreasing image blurring. This image assessment is subjective, and the individual radiologist preference for this synthetic appearance may vary, particularly with increasing exposure to and clinical experience with these types of images.

In this study, quantitative assessment of image quality was not performed. Calculation of parameters such as SNR in the context of parallel imaging is technically difficult and usually not feasible clinically; further, these complexities are even more challenging when compressed sensing is introduced. Thus, subjective image quality and delineation of abdominal anatomical structures were thoroughly evaluated in a clinical setting. However, arguably these subjective assessments, along with diagnostic accuracy, are ultimately more relevant to clinical adoption of an imaging method.

The qualitative assessments in the study were subjective: different readers may have different interpretation of the scoring criteria of the image assessment, especially for overall image quality. For example, because a variable density sampling pattern was used, the resulting image resolution of a parallel imaging reconstruction compared to compressed sensing reconstruction was not clearly predictable, and radiologists' perception of image blurring and resolution is subjective. Unfortunately, to understand the impact of compressed sensing reconstruction on image resolution, phantom studies may not be applicable because the phantoms are usually much sparser than in vivo images. Fully sampled arterial phase in vivo datasets could be more ideal, but are impossible to acquire for contrast-enhanced abdominal MRI due to contrast passage during the long time (>2 minutes) to acquire a high spatial resolution fully-sampled dataset. However, with clearly defined criteria, the evaluation of delineation of specific anatomical structures is arguably more practical to

assess these images. From Figure 3, Figure 4 and Table 8, we can see a much better inter-observer agreement for the delineation of anatomical structures, where the scoring criteria is defined less subjectively, than for overall image quality assessment.

The study cohort was a heterogeneous patient population, which included patients with abdominal tumors (hepatocellular carcinoma, Wilms tumor, benign liver tumors), a ventricular mass, and solid-organ transplants. The benefit of including patients with multiple and diverse clinical conditions is the assessment of the feasibility of using CC-L_1-SPIRiT in various clinical circumstances. However, further validation should be directed towards specific patient population with specific diseases.

One limitation of our study was that the acceleration factor was fixed in this study. At this high acceleration of 7.2, compressed sensing reconstructions clearly improved image quality and anatomical structures were better delineated. This lends evidence that this approach to imaging may be acceptable for clinical examinations in a pediatric setting. However, we did not perform the study at lower and higher accelerations. Therefore, further studies should be performed using different acceleration factors, enabling determination of the factor at which the reconstruction deteriorates to an unacceptable degree.

Anatomical structures routinely evaluated on abdominal MRI exams were clearly delineated with compressed sensing reconstructions. In addition, pathological lesions, like bone lesions and abdominal tumors were well delineated with CC-L_1-SPIRiT compared with ARC. However, given the small sample sizes of patients with any specific lesion, our study does not address the diagnostic accuracy of using a compressed sensing and coil compression for any particular imaging indication.

Acknowledgments

The authors thank Prof. Brian Hargreaves for valuable discussions.

Grant Sponsors: This work was supported by NIH grants R01 EB009690, P41 EB015891, John & Tashia Morgridge Faculty Scholars Fund, and GE Healthcare.

References

1. Olsen OE. Imaging of abdominal tumours: CT or MRI? Pediatr Radiol. 2008; 38(Suppl 3):452–458. [PubMed: 18265967]
2. Darge K, Anupindi SA, Jaramillo D. MR imaging of the abdomen and pelvis in infants, children, and adolescents. Radiology. 2011; 261:12–29. [PubMed: 21931139]
3. Vasanawala SS, Lustig M. Advances in pediatric body MRI. Pediatr Radiol. 2011; 41(Suppl 2):549–554. [PubMed: 21847737]
4. Sury MR, Smith JH. Deep sedation and minimal anesthesia. Paediatr Anaesth. 2008; 18:18–24. [PubMed: 18095961]
5. Pruessmann KP, Weiger M, Scheidegger MB, Boesiger P. SENSE: sensitivity encoding for fast MRI. Magn Reson Med. 1999; 42:952–962. [PubMed: 10542355]
6. Griswold MA, Jakob PM, Heidemann RM, et al. Generalized autocalibrating partially parallel acquisitions (GRAPPA). Magn Reson Med. 2002; 47:1202–1210. [PubMed: 12111967]
7. Roemer PB, Edelstein WA, Hayes CE, Souza SP, Mueller OM. The NMR phased array. Magn Reson Med. 1990; 16:192–225. [PubMed: 2266841]
8. Donoho D. Compressed sensing. IEEE Trans Inf Theory. 2006; 52:1289–1306.

9. Lustig M, Donoho D, Pauly JM. Sparse MRI: the application of compressed sensing for rapid MR imaging. Magn Reson Med. 2007; 58:1182–1195. [PubMed: 17969013]
10. Liang D, Liu B, Wang J, Ying L. Accelerating SENSE using compressed sensing. Magn Reson Med. 2009; 62:1574–1584. [PubMed: 19785017]
11. Vasanawala SS, Alley MT, Hargreaves BA, Barth RA, Pauly JM, Lustig M. Improved pediatric MR imaging with compressed sensing. Radiology. 2010; 256:607–616. [PubMed: 20529991]
12. Vasanawala, SS.; Murphy, MJ.; Alley, MT., et al. Practical parallel imaging compressed sensing MRI: Summary of two years of experience in accelerating body MRI of pediatric patients. Proceedings of IEEE Int Symp Biomed Imag; Chicago. 2011. p. 1039-1043.
13. Brau AC, Beatty PJ, Skare S, Bammer R. Comparison of reconstruction accuracy and efficiency among autocalibrating data-driven parallel imaging methods. Magn Reson Med. 2008; 59:382–395. [PubMed: 18228603]
14. Murphy M, Alley M, Demmel J, Keutzer K, Vasanawala S, Lustig M. Fast L_1-SPIRiT compressed sensing parallel imaging MRI: scalable parallel implementation and clinically feasible runtime. IEEE Trans Med Imaging. 2012; 31:1250–1262. [PubMed: 22345529]
15. Vasanawala, S.; Grafendorfer, T.; Calderon, P., et al. Millimeter isotropic resolution volumetric pediatric abdominal MRI with a dedicated 32 channel phased array coil. Proceedings of the 19th Annual Meeting of ISMRM; Montreal. 2011. p. 161
16. McDougall MP, Wright SM. 64-channel array coil for single echo acquisition magnetic resonance imaging. Magn Reson Med. 2005; 54:386–392. [PubMed: 16032696]
17. Schmitt M, Potthast A, Sosnovik DE, et al. A 128-channel receive-only cardiac coil for highly accelerated cardiac MRI at 3 Telsa. Magn Reson Med. 2008; 59:1431–1439. [PubMed: 18506789]
18. Buehrer M, Pruessmann KP, Boesiger P, Kozerke S. Array compression for MRI with large coil arrays. Magn Reson Med. 2007; 57:1131–1139. [PubMed: 17534913]
19. Huang F, Vijayakumar S, Li Y, Hertel S, Duensing GR. A software channel compression technique for faster reconstruction with many channels. Magn Recon Imaging. 2008; 26:133–141.
20. Zhang T, Pauly JM, Vasanawala SS, Lustig M. Coil compression for accelerated imaging with Cartesian sampling. Magn Reson Med. 2013; 69:571–582. [PubMed: 22488589]
21. Lustig M, Pauly JM. SPIRiT: iterative self-consistent parallel imaging reconstruction from arbitrary k-space. Magn Reson Med. 2010; 64:457–471. [PubMed: 20665790]
22. Alley, MT.; Murphy, MJ.; Keutzer, K., et al. Improved time-resolved, 3D phase contrast imaging through variable Poisson sampling and partial respiratory triggering. Proceedings of the 19th Annual Meeting of ISMRM; Montreal. 2011. p. 1218
23. Beatty, P.; Brau, A.; Chang, S., et al. A method for autocalibrating 2-D accelerated volumetric parallel imaging with clinically practical reconstruction times. Proceedings of the 15th Annual Meeting of ISMRM; Berlin. 2007. p. 1749

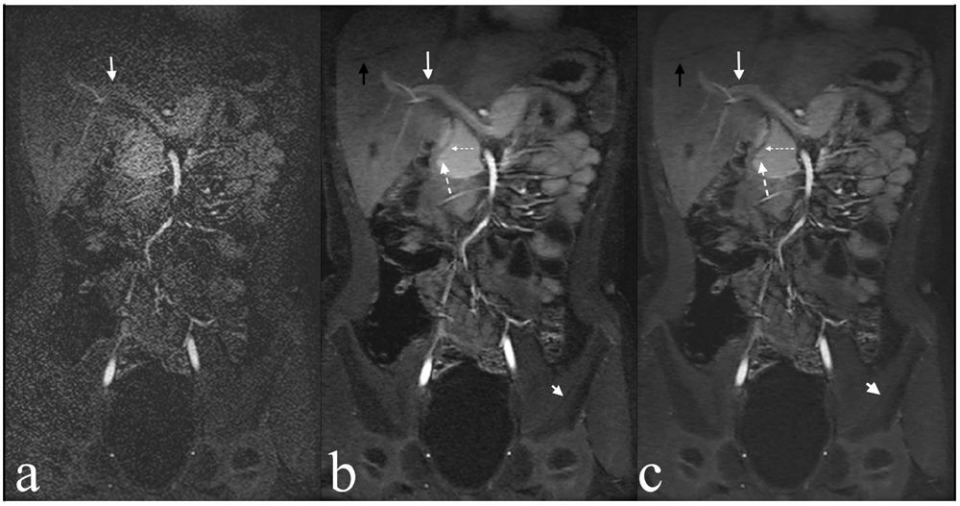

Figure 1.

Example of ARC (a), L_1-SPIRiT (b), and CC-L_1-SPIRiT (c) reconstructions of a 6-year-old female. Note delineation of hepatic vein branch (black arrow), portal vein (white arrow), pancreatic duct (large dashed arrow), bile duct (small dashed arrow), and cortex of left iliac bone (short white arrow).

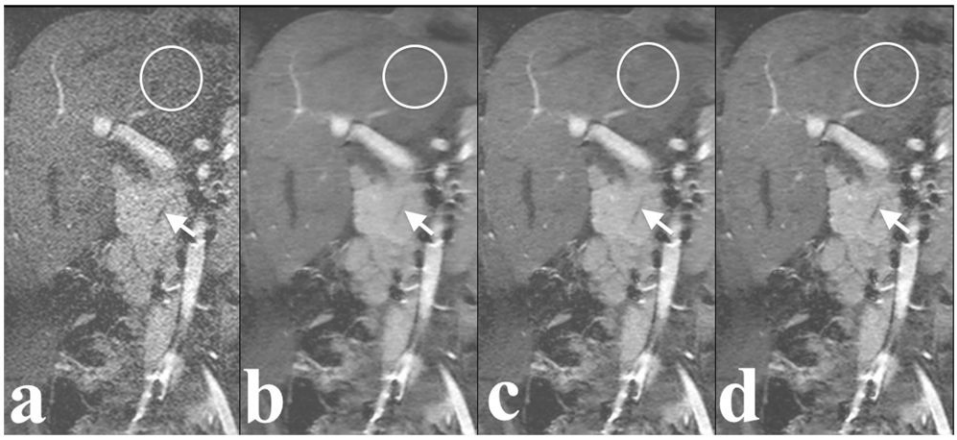

Figure 2.

Example of ARC reconstruction (a), L_1-SPIRiT reconstruction with the default reconstruction parameters (b), L_1-SPIRiT reconstruction with adjusted reconstruction parameters (c), and CC-L_1-SPIRiT reconstruction with the default reconstruction parameters (d) of a 6-year-old female. Note delineation of pancreatic duct (arrow). L_1-SPIRiT reconstruction with the default reconstruction parameters has a synthetic appearance, which is reflected by the circled cartoon-like almost “noiseless” liver. The synthetic appearance was removed with adjusted reconstruction parameters.

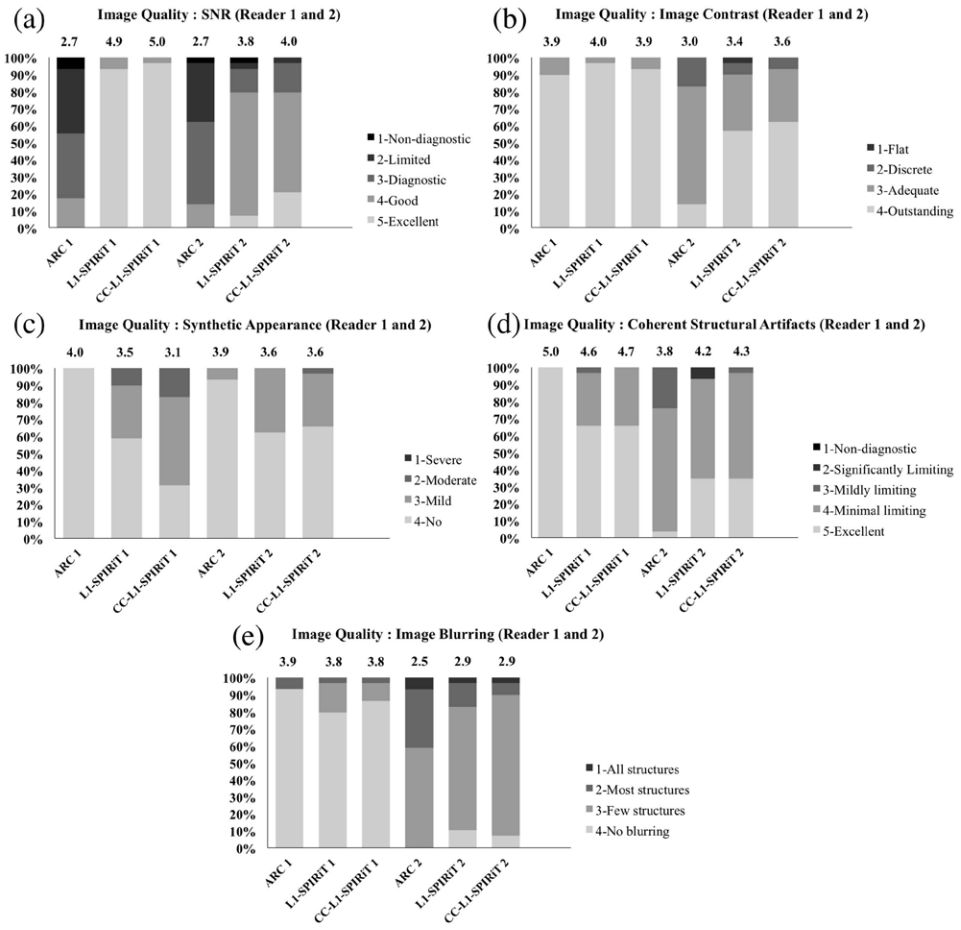

Figure 3.

Representative results of overall image quality assessments for ARC, L_1-SPIRiT and CC-L_1-SPIRiT reconstructions for Reader 1 and Reader 2: (a) Qualitative SNR; (b) Image contrast; (c) Synthetic appearance; (d) Coherent structural artifacts; and (e) Image blurring. Each color bar represents the percentage of number of the cases with the same score. The mean score of each reconstruction is shown on top of the color bar.

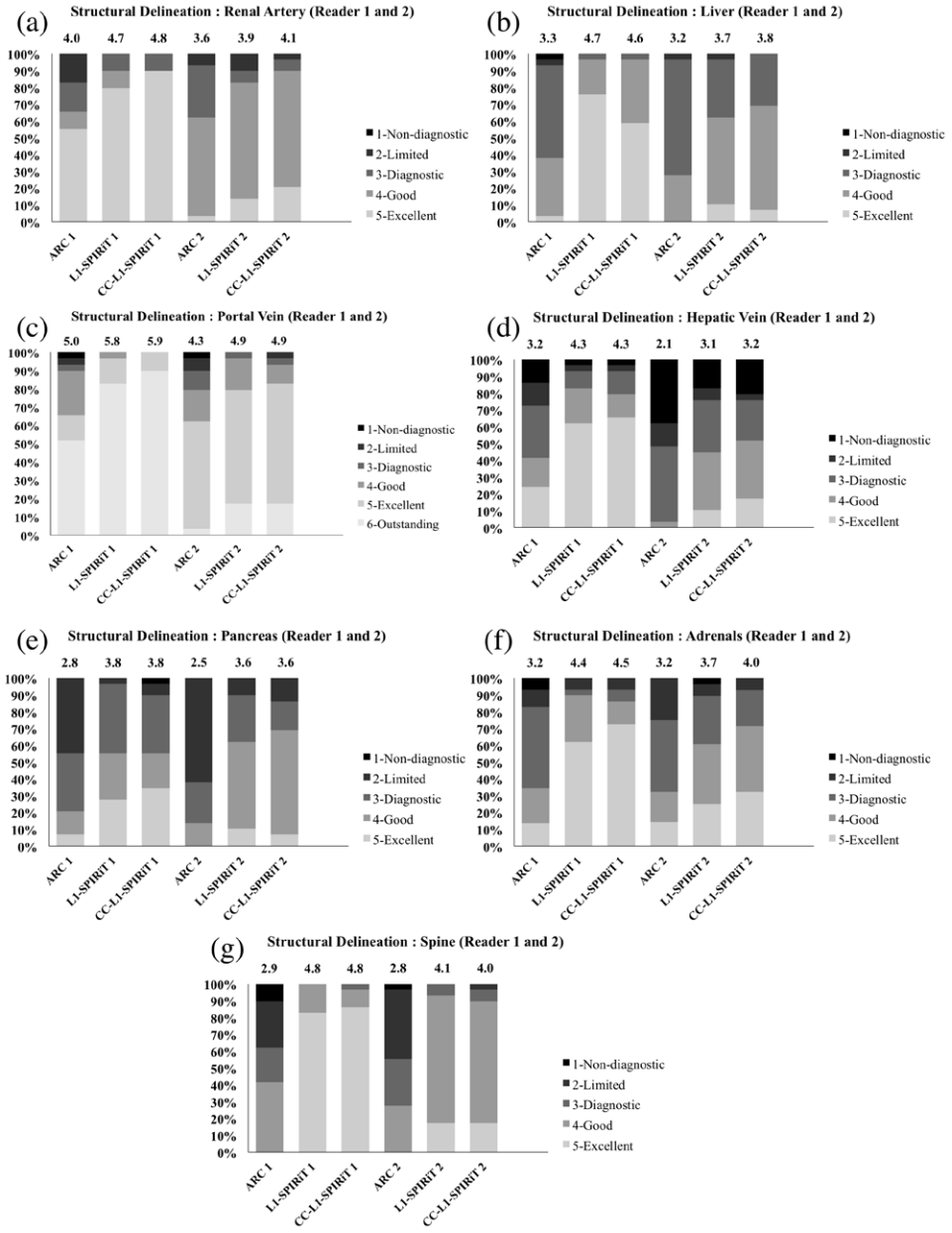

Figure 4.

Representative results of the delineation of anatomical structures for ARC, L_1-SPIRiT and CC-L_1-SPIRiT reconstructions for Reader 1 and Reader 2: (a) Renal artery; (b) liver; (c) Portal vein; (d) Hepatic vein; (e) pancreas; (f) adrenals and (g) spine. Each color bar represents the percentage of number of the cases with the same score. The mean score of each reconstruction is shown on top of the color bar.

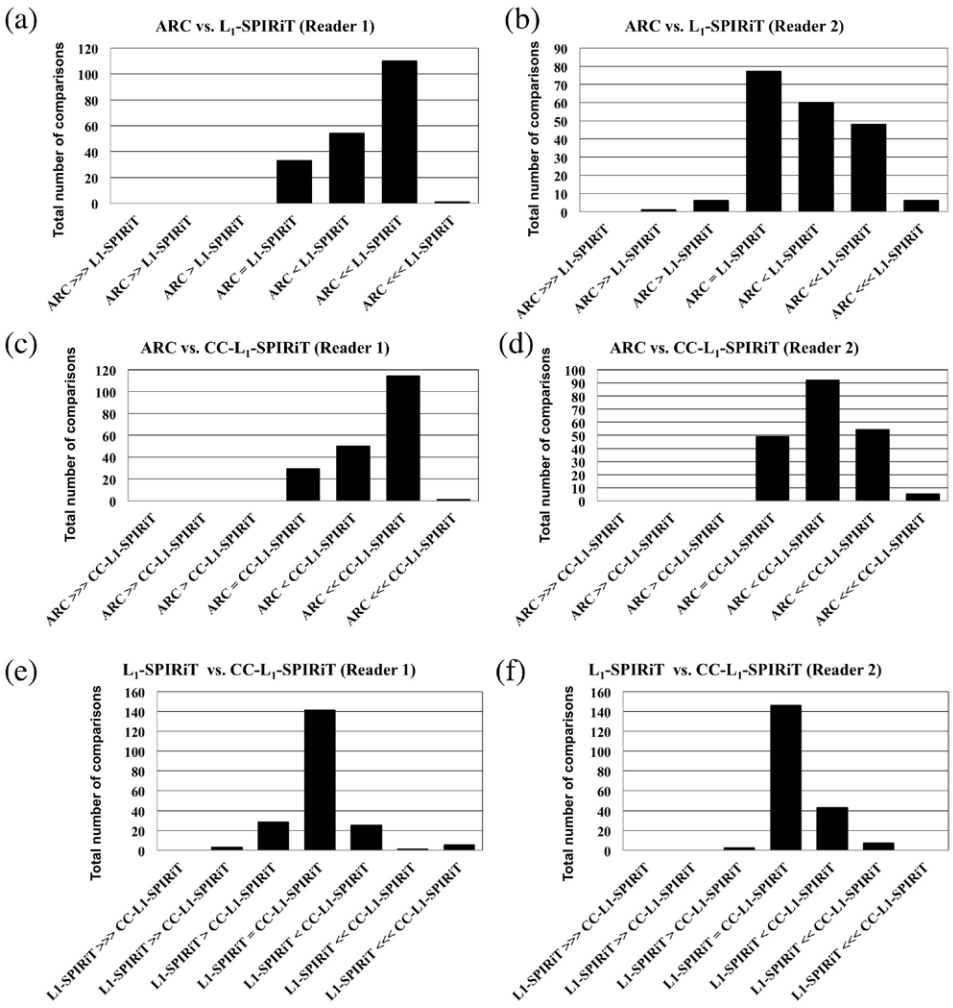

Figure 5.

Representative results of the paired assessment of structural delineation based on the scoring criteria in Tab. 4. Bar graphs were generated based on the comparisons of all seven anatomical structures. The scores of the comparisons (-3, -2, -1, 0, 1, 2, 3) were represented by (⋙, ≫, >, =, <, ≪, ⋘) respectively in the bar graph. For example, "ARC > L_1-SPIRiT" means that there was aesthetic improvement in ARC than L_1-SPIRiT. The comparison results between ARC and L_1-SPIRiT are shown in (a) and (b) for reader 1 and reader 2 respectively. The comparison results between ARC and CC-L_1-SPIRiT are shown in (c) and (d). The comparison results between L_1-SPIRiT and CC-L_1-SPIRiT are shown in (e) and (f).

Table 1

Demographics of patients, acquisition parameters, reconstruction times and clinical indications.

Subject number	Age (years)	Gender	Slice Thickness (mm)	S/I FOV (cm)	In-plane Matrix	L_1-SPIRiT Reconstruction Time (s)	CC-L_1-SPIRiT Reconstruction Time (s)
1	2.75	M	1	26	320×320	267	34
2	3.92	M	1	30	320×320	242	33
3	0.67	F	1	24	320×320	276	37
4	5.5	F	1	30	320×320	263	33
5	5.75	F	1	32	320×320	285	36
6	6.42	F	1	28	320×320	364	48
7	4.5	F	1	28	320×320	263	37
8	3.33	F	1	28	320×320	289	40
9	2.42	M	0.8	28	288×288	329	45
10	5.33	M	0.8	30	288×288	307	40
11	4.25	F	1	26	288×288	330	44
12	3.67	M	0.8	24	288×288	261	34
13	3.75	M	0.8	28	288×288	356	41
14	3.25	M	1	24	288×288	254	39
15	0.25	F	1	20	320×320	359	41
16	9	M	1	32	320×320	336	39
17	2.25	M	1	28	320×320	321	43
18	1.08	F	1	26	320×320	282	45
19	3.75	F	1	28	320×320	209	31
20	3.08	M	1	34	320×320	203	31
21	0.92	F	1	26	320×320	202	28
22	3.92	M	1	28	320×320	258	35
23	5	M	0.8	28	320×320	342	38
24	1.25	F	1	28	320×320	213	30
25	6	M	1	30	320×320	214	30
26	2.5	F	1	28	320×320	214	31
27	1.92	F	1	28	320×320	302	34
28	6.92	M	1	32	320×320	228	33

Subject number	Age (years)	Gender	Slice Thickness (mm)	S/I FOV (cm)	In-plane Matrix	L_1-SPIRiT Reconstruction Time (s)	CC-L_1-SPIRiT Reconstruction Time (s)
29	6.58	F	1	30	320×320	211	31

Table 2

Scoring Criteria for Individual Assessments of Overall Image Quality*

Score	Qualitative SNR	Image Contrast	Synthetic Appearance	Coherent Structural Artifact	Image Blurring
1	Non-diagnostic	Flat (Very little contrast between arterial structures and background)	Severe synthetic appearance	Non-diagnostic	Blurring of all structures
2	Somewhat limiting	Discrete (No gradation)	Moderate synthetic appearance	Significantly limiting artifact	Blurring of most structures
3	Adequate for most structures	Adequate (Gradation can be seen just in low intensity or high intensity objects)	Mild synthetic appearance	Mildly limiting artifact	Blurring of few structures
4	More than adequate for most structures	Outstanding (Gradation can be seen in both low intensity and high intensity objects)	No synthetic appearance	Minimal limiting artifact	No blurring of any structures
5	More than adequate for all structures	-	-	No Artifact	-

* Images with individual assessment score equal or greater than 3 are considered to be diagnostically acceptable, and less than 3 are considered to be diagnostically non-acceptable.

Table 3

Scoring Criteria for Delineation of Anatomical Structures

Score	Renal Arteries	Liver	Portal Veins	Hepatic Veins	Pancreas	Adrenals	Spine
1 (Non-diagnostic)	Poorly seen	Lesions larger than 2 cm can be assessed	Central portal vein can not be assessed	Central hepatic vein can not be assessed	Heterogeneous signals and contours not defined	Adrenals can not be assessed	Vertebrae from disc can not be separated
2 (Limited)	Seen but not confident for stenosis assessment	Lesions larger than 5mm can not be assessed	Left or right portal vein can not be assessed	Left, right and middle hepatic veins can be seen	Homogenous signals or contours defined	Margins and mass of adrenals can be seen but not confident	Most of the vertebrae or disc can be seen
3 (Diagnostic)	Confident in the margins of renal artery and accessory renal arteries	Some lesions larger than 5mm can be assessed	Both left and right portal vein can be assessed	Branch hepatic veins can be seen	Homogenous signals and contours defined	margins and mass of adrenals can be seen	Most of the vertebrae and disc can be seen
4 (Good)	First order branches of renal arteries are sharply delineated	All lesions larger than 5mm can be assessed	Some second order branches can be assessed	Branch hepatic veins can be seen sharply	Homogenous signals; contours defined; Pancreatic duct partly seen	Most of the margins are clearly defined	All the vertebrae and disc can be seen
5 (Excellent)	Up to second order branches of renal arteries are sharply delineated	Lesions larger than 2mm can be assessed	All second order branches can be assessed	Branch hepatic veins to within 1 cm of capsule can be seen	Can see entire pancreatic duct (from tail to ampulla)	All the margins are well defined	All the vertebrae and disc can be seen; growth plate sharply defined
6 (Outstanding)	-	-	Vessels to within 1 mm of capsule can be assessed	-	-	-	-

Table 4

Scoring Criteria for Paired Side-by-side Assessments of Quality of Structural Delineation*

Score	Quality of Structural Delineation (Left vs. Right)
-3	Structures seen on the left but not on the right
-2	Better delineated on the left than on the right
-1	Aesthetic improvement on the left
0	Equivalent
1	Aesthetic improvement on the right
2	Better delineated on the right than on the left
3	Structures seen on the right but not no the left

* One reconstruction was presented on the left side of the screen and the other on the right side in a randomized blinded fashion for comparisons. For quality of structural delineation, structures evaluated were renal artery and branches, liver, portal vein and branches, hepatic vein and branches, pancreatic duct, adrenal, spine, and lesion. Structures on both sides were evaluated unless absent.

Table 5

Individual Assessments of Overall Image Quality: the proportion with diagnostically acceptable image quality for each reconstruction is shown (29 cases).

Overall Image Quality	Number of cases (proportions) Reader 1			Number of cases (proportions) Reader 2		
	ARC	L_1-SPIRiT	CC-L_1-SPIRiT	ARC	L_1-SPIRiT	CC-L_1-SPIRiT
Qualitative SNR	16 (55%)	29 (100%)	29 (100%)	18 (62%)	27 (93%)	28 (97%)
Image contrast	29 (100%)	29 (100%)	29 (100%)	24 (83%)	26 (90%)	27 (93%)
No Synthetic appearance	29 (100%)	26 (90%)	24 (83%)	29 (100%)	29 (100%)	28 (100%)
No Structural coherent artifacts	29 (100%)	29 (100%)	29 (100%)	29 (100%)	27 (93%)	29 (100%)
No Image blurring	28 (97%)	28 (97%)	28 (97%)	17 (59%)	24 (83%)	26 (90%)

Table 6

Mean scores of qualitative image assessments and delineation of anatomical structures, and the paired Wilcoxon ranked sum test between ARC and L_1-SPIRiT, ARC and CC-L_1-SPIRiT, and L_1-SPIRiT and CC-L_1-SPIRiT (when reconstructed images were assessed individually)*

	Mean Scores (Reader1/Reader2)			P values of the Wilcoxon test (Reader 1/Reader2)		
	ARC	**L_1-SPIRIT**	**CC-L_1-SPIRiT**	**ARC vs L_1-SPIRiT**	**ARC vs CC-L_1-SPIRiT**	**L_1-SPIRiT vs CC-L_1-SPIRiT**
Qualitative Image Assessments						
Qualitative SNR	2.7/2.7	4.9/3.8	5.0/4.0	**<0.05/<0.05**	**<0.05/<0.05**	1.0/0.14
Coherent Structural Artifacts	5.0/3.8	4.6/4.2	4.7/4.3	**<0.05/<0.05**	**<0.05/<0.05**	0.79/0.46
Image Contrast	3.9/3.0	4.0/3.4	3.9/3.6	0.35/**<0.05**	1.0/**<0.05**	0.35/0.34
Image Blurring	3.9/2.5	3.8/2.9	3.8/2.9	**<0.05/<0.05**	0.15/**<0.05**	0.42/0.77
Synthetic Appearance	4.0/3.9	3.5/3.6	3.1/3.6	**<0.05/<0.05**	**<0.05/<0.05**	**<0.05**/1.0
Delineation of Anatomical Structures						
Renal Artery	4.0/3.6	4.7/3.9	4.8/4.1	**<0.05**/0.06	**<0.05/<0.05**	0.34/0.17
Liver	3.3/3.2	4.7/3.7	4.6/3.8	**<0.05/<0.05**	**<0.05/<0.05**	0.07/0.62
Portal Veins	5.0/4.3	5.8/4.9	5.9/4.9	**<0.05/<0.05**	**<0.05/<0.05**	0.34/1.0
Hepatic Veins	3.2/2.1	4.3/3.1	4.3/3.2	**<0.05/<0.05**	**<0.05/<0.05**	1.0/0.49
Pancreas	2.8/2.5	3.8/3.6	3.8/3.6	**<0.05/<0.05**	**<0.05/<0.05**	0.82/1.0
Adrenals	3.2/3.2	4.4/3.7	4.5/4.0	**<0.05/<0.05**	**<0.05/<0.05**	0.81/0.11
Spine	2.9/2.8	4.8/4.1	4.8/4.0	**<0.05/<0.05**	**<0.05/<0.05**	1.0/0.53

*P<0.05 was considered as a statistically significant level (shown in bold)

Table 7

Paired assessment of delineation of anatomical structures. The number of cases with preference for ARC, L_1-SPIRiT, or CC-L_1-SPIRiT when compared in pairs is shown for each anatomical structure using the criteria in Table 4. Note cells with zero cases are left blank in the table.*

	ARC vs L_1-SPIRiT							ARC vs CC-L_1-SPIRiT							L_1-SPIRiT vs CC-L_1-SPIRiT						
score	**-3**	**-2**	**-1**	**0**	**1**	**2**	**3**	**-3**	**-2**	**-1**	**0**	**1**	**2**	**3**	**-3**	**-2**	**-1**	**0**	**1**	**2**	**3**
Renal Artery																					
Reader 1				7	12	10					7	16	6					26	3		
			P < 0.05							**P < 0.05**							P = 0.15				
Reader 2			1	16	9	3					12	15	2					23	5	1	
			P < 0.05							**P < 0.05**							**P < 0.05**				
Portal Vein																					
Reader 1				2	9	18						5	23	1			6	18	5		
			P < 0.05							**P < 0.05**							P = 0.80				
Reader 2			1	11	10	6	1				3	22	4					20	8	1	
			P < 0.05							**P < 0.05**							**P < 0.05**				
Hepatic Vein																					
Reader 1				2	5	22					2	6	20	1		1	5	19	4		
			P < 0.05							**P < 0.05**							P = 0.44				
Reader 2			2	7	9	8	3				4	10	14	1			1	22	5	1	
			P < 0.05							**P < 0.05**							P = 0.07				
Pancreas																					
Reader 1				16	5	8					15	4	8	2			1	22	5	1	
			P < 0.05							**P < 0.05**							P = 0.07				
Reader 2		1	2	9	11	5	1				8	16	4	1				18	9	2	
			P < 0.05							**P < 0.05**							**P < 0.05**				
Adrenals																					
Reader 1				6	15	8					4	14	11				3	21	5		
			P < 0.05							**P < 0.05**							P = 0.53				
Reader 2				22	5	1	1				14	12	3					22	6	1	
			P < 0.05							**P < 0.05**							**P < 0.05**				
Spine																					

	ARC vs L_1-SPIRiT							ARC vs CC-L_1-SPIRiT							L_1-SPIRiT vs CC-L_1-SPIRiT						
score	**-3**	**-2**	**-1**	**0**	**1**	**2**	**3**	**-3**	**-2**	**-1**	**0**	**1**	**2**	**3**	**-3**	**-2**	**-1**	**0**	**1**	**2**	**3**
Reader 1						28	1						28	1		2	9	16	2		
				P < 0.05							**P < 0.05**							**P < 0.05**			
Reader 2				2	5	22						6	22	1			1	20	7	1	
				P < 0.05							**P < 0.05**							**P < 0.05**			
Lesions																					
Reader 1					8	16					1	5	18				4	19	1		
				P < 0.05							**P < 0.05**							P = 0.23			
Reader 2				10	11	3					8	11	5					21	3		
				P < 0.05							**P < 0.05**							P = 0.15			

*P<0.05 was considered as a statistically significant level (shown in bold)

Table 8

Inter-observer agreement results using weighted kappa coefficients between Reader 1 and Reader 2 for overall image quality assessments and delineation of anatomical structures for ARC, L_1-SPIRiT and CC-L_1-SPIRiT.*

	ARC	L_1-SPIRiT	CC-L_1-SPIRiT
Overall Image Quality			
Qualitative SNR	Fair	Slight	Slight
Coherent Structural Artifacts	Slight	Poor	Slight
Image Contrast	Poor	Poor	Poor
Image Blurring	Slight	Fair	Fair
Synthetic Appearance	Slight	Poor	Slight
Delineation of Anatomical Structures			
Renal Artery	Fair	Moderate	Fair
Liver	Moderate	Fair	Slight
Portal Vein	Moderate	Slight	Poor
Hepatic Vein	Fair	Fair	Moderate
Pancreas	Fair	Substantial	Substantial
Adrenals	Substantial	Moderate	Substantial
Spine	Substantial	Slight	Slight

* Interpretation of weighted kappa coefficient (kw) used: kw<0, poor; 0<=kw<0.2, slight; 0.2<=kw<0.4, fair; 0.4<=kw<0.6, moderate; 0.6<=kw<0.8, substantial; 0.8<=kw<1, almost perfect.